Activation of hTREK-1 by polyunsaturated fatty acids does not only involve membrane tension

Emilie BECHARD[1], Elodie AREL[1], Jamie BRIDE[1], Julien LOURADOUR[1], Xavier BUSSY[1], Anis ELLOUMI[2], Claire VIGOR[2], Pierre SOULE[4], Camille OGER[2], Jean-Marie GALANO*[2], Thierry DURAND*[2], Jean-Yves LE GUENNEC*[1], Hamid MOHA-OU-MAATI*[3], Marie DEMION*[$,1].

[1]: PhyMedExp, Université de Montpellier, Inserm U1046, UMR CNRS 9412, Montpellier (France)
[2]: IBMM, Université de Montpellier, UMR CNRS 5247, ENSCM, Montpellier (France)
[3]: IGF, Université de Montpellier, Inserm 1191, UMR CNRS 5203, Montpellier (France) Present adress INM, Inserm U1298, Montpellier (France)
[4] : NanoTemper Technologies GmbH, Munich (Germany)
* : last co-authors

[$]corresponding author
Marie DEMION
PhyMedExp, Inserm U1046, CNRS UMR9214
CHU Arnaud de Villeneuve
Bâtiment Craste de Paulet
370 avenue du Doyen Gaston Giraud
34290 MONTPELLIER Cedex 05
France

Running title : hTREK-1 is directly activated by PUFAs

ABSTRACT

TREK-1 is a mechanosensitive channel also activated by polyunsaturated fatty acids (PUFAs). In this study, we compared the effect of multiple fatty acids and ML402. First, we showed a variable TREK-1 activation by PUFAs related to the variable constitutive activity of TREK-1. Then, we observed no correlation between TREK-1 activation and acyl chain length or number of double bonds suggesting that the bilayer-couple hypothesis cannot explain by itself the activation of TREK-1 by PUFAs. The membrane fluidity measurement is not modified by PUFAs at 10 µM. The spectral shift analysis in TREK-1-enriched microsomes indicates a $K_{D,TREK1}$ at 44 µM of C22:6 n-3. PUFAs display the same activation and reversible kinetics than the direct activator ML402 and activate TREK-1 in both whole-cell and inside-out configurations of patch-clamp suggesting that the binding site of PUFAs is accessible from both sides of the membrane, as for ML402. Finally, we proposed a two steps mechanism for TREK-1 activation by PUFAs: first, insertion into the membrane, without fluidity or curvature modifications, and then interaction with TREK-1 channel to open it.

INTRODUCTION

Potassium channels have a crucial role in the electrical activity of excitable cells such as neurons and cardiomyocytes. Some of these potassium channels are common drug targets modulating the action potential shape and consecutively organs functions. Among the K^+ channels, members of the two-pore domains K^+ channels family (K2P) are involved in the repolarization phase of action potential and in the resting membrane potential (Kelly *et al*, 2006). K2P family includes 15 members classified in 6 functional subfamilies: TWIK (Tandem of pore domains in a Weak Inward rectifying K channel), TREK (TWIK-Related K channel), TASK (TWIK-related Acid Sensitive K channel), TALK (TWIK-related Alkaline pH-activated K channel), THIK (Tandem pore domain Halothane-Inhibited K channel),

TRESK (TWIK-Related Spinal Cord K Channel). K2P channels share common structural features, each subunit containing two-pore domains (P1, P2) and four putative transmembrane segments (M1-M4) (Honoré, 2007). The dimerization of K2P channels allows the formation of the canonical K^+ selective pore domain. TREK-1 channel, one of the three members of the TREK subfamily with TREK-2 and TRAAK, has been discovered in 1996 by Fink *et al*. The gating of TREK-1 channel is poly-modulated by a wide range of physical and chemical stimuli including mechanical stretch, temperature, voltage, pH changes, pharmacological agents and polyunsaturated fatty acids (PUFAs). This channel is widely studied since its activation is involved in neuroprotection (Lamas & Fernández-Fernández, 2019), cardioprotection (Kamatham *et al*, 2019), analgesia (Li & Toyoda, 2015) and reduced epilepsy crisis (Heurteaux *et al*, 2004). In the majority of these diseases, the protection afforded by TREK-1 activation is due to the hyperpolarization of the membrane potential (Djillani *et al*, 2019)

Among the wide diversity of TREK-1 modulators, PUFAs have been shown to behave as strong activators (Patel *et al*, 1998; Danthi *et al*, 2003). PUFAs are amphipathic molecules with a hydrophilic carboxyl head and a long hydrophobic chain of carbons and multiple double bonds. The two main classes of PUFAs are n-3-PUFAs and n-6-PUFAs based on the position of the first double bond from the carbon ω starting at the methyl extremity. Numerous studies suggest that n-3-PUFAs, such as docosahexaenoic acid (DHA) and eicosapentaenoic acid (EPA), exert antiarrhythmic properties through the modulation of ionic channels and consequent membrane hyperpolarization (Kang & Leaf, 1994, 1996). Such hyperpolarization could be consecutive to TREK-1 activation as it is largely expressed in the myocarde(Wiedmann *et al*, 2021; Bechard *et al*, 2022). Since TREK channels are mechano-sensitives, the comparison of the effects of different PUFAs on TRAAK (Fink *et al*, 1996) suggests that PUFAs can insert inside the membrane inducing an increase in membrane

fluidity (Leifert *et al*, 1999) that in turn modifies membrane curvature and tension (Sheetz and Singer., 1974). In fact, TRAAK is very likely to be activated by PUFAs through this mechanosensitive pathway since the activation is related to the acyl chain length and to the number of double bonds (Fink et al., 1998; Maingret *et al*, 1999; Patel et al., 2001; Honoré, 2007). However, while it is known that PUFAs also activate TREK-1 channel, no study has compared the effects of different PUFAs on TREK-1 to determine a potential mechanism of action. Here, we propose a study that allows a better understanding of which features of PUFAs are essential for their effects on TREK-1. We performed a thorough comparison of the effects of 9 PUFAs (from 18 to 22 carbons with 2 to 6 double bonds) and 2 other C18 FA (mono-unsaturated and saturated) on the TREK-1 current (I_{TREK-1}). We report that there is no correlation between the acyl chain length and TREK-1 activation, as for the PUFAs-induced membrane fluidity. Then, the comparison of the effects of PUFAs and ML402, a direct activator of TREK-1 binding within a cryptic pocket behind the selectivity filter (Lolicato *et al*, 2017), suggests that there is a at least one binding site for PUFAs on TREK-1 channel. This hypothesis is reinforced by the affinity protein-PUFA test performed in TREK-1 enriched-microsomes using the nanotemper technology, but the precise binding site remains to be determined in further studies.

RESULTS

TREK-1 channel activation by PUFAs does not depend of acyl chain length

As previously described,TREK-1 channel is activated by PUFAs, such as arachidonic acid (AA, C20:4 n-6) (Patel *et al*, 1998), LA (Danthi *et al*, 2003) or DHA (Ma & Lewis, 2020). In our hands, the average membrane potential (Em) of HEK hTREK-1 cells was -69.2 ± 0.7 mV (mean ± SEM) (**Fig 1D**, n=130), with a variable initial current density of 15.3 ± 1.2 pA/pF (n=130) at 0 mV. During PUFA superfusion, the current density elicited by voltage ramp from -100 mV to +30 mV progressively increased until a steady-state was reached (**Fig 1A and 1B**). When TREK-1 is activated, Em hyperpolarized to -81.7 ± 0.3 mV (**Fig 1D**, n=130), close to the theorical equilibrium potential of K^+ ions (E_K = -86.5 mV). In order to determine wether the variability of the initial current density (I_0) was related to a variability of TREK-1 channel activity in initial condition, we superfused an inhibitor of TREK-1 channel, Norfluoxetine (NrFlx) at 10 µM. As the initial current was significantly decrease from 8.8 ± 2.2 pA/pF to 3.7 ± 0.9 pA/pF (p-value=0.02; n=5) when Norfluoxetine was applied and as the characteristic outward rectification of I_{TREK-1} was lost, we concluded that I_0 was carried out mostly by TREK-1 channel (**Fig 1C**).

To investigate the importance of the acyl chain length and double bounds, we compared the response of 9 PUFAs with various chain lengths, from 18 to 22 carbons with different number of double bounds, from 2 to 6 unsaturations (**Table 1**). We plotted the relationship between current density at 0 mV in the presence of PUFA (I_{PUFA}) normalized to the initial current density (I_0)(this normalized parameter corresponds to the current fold-increase (I_{PUFA}/I_0)) and the number of carbons on the acyl chain. As shown in **Fig 1E**, there is no correlation between PUFA activation I_{PUFA}/I_0 and the acyl chain length (Spearman correlation test : p-value = 0.19), as for the current density of TREK-1 channel after PUFA perfusion (Spearman correlation test : p-value = 0.10) (**Fig 1G**). We then plotted the relationship between I_{PUFA}/I_0

121 at 0 mV or current density in response of PUFA perfusion and the number of double bounds
122 in the acyl chains and also observed no correlation (**Fig 1F and Fig 1H**; Spearman correlation
123 tests: p-value = 0.63 and p-value = 0.56 respectively). These data reveal that there is no
124 relationship between the effect of PUFAs on TREK-1 and the acyl chain length or the number
125 of double bonds. Indeed, C22:6 n-3 tends to have a stronger effect than C22:5 n-3 on TREK-1
126 current, while they share the same number of carbons (**Fig 1E-H** and **Table 1**). Accordingly,
127 the most potent activators were both one of the shortest one, C18:2 n-6 (I_{PUFA}/I_0 = 24.8 ± 3.3;
128 current density = 353.7 ± 22.4 pA/pF), and one of the longest one, C22:6 n-3 (I_{PUFA}/I_0 = 29.8
129 ± 4.4; current density = 276.8 ± 24.5 pA/pF). Conversely, C18:2 n-6 is one of the most potent
130 activator but C18:3 n-3 failed to activate TREK-1 channel (I_{PUFA}/I_0 = 1.4 ± 0.1; Current
131 density = 20.7 ± 4.2 pA/pF). Like C18:3 n-3, the saturated stearic acid (C18:0) had no effect
132 on TREK-1 while the mono-unsaturated C18:1 n-9 produced a 7.4 ± 1.9-fold increase of
133 I_{TREK-1} (n=12, **Table 1**). However, statistical analysis failed to discriminate the PUFA's
134 effects (I_{PUFA}/I_0 parameters compared with a nonparametric kruskall-wallis test) probably due
135 to the important variability of the effects.
136
137 **The variability in PUFA responses is related to the variable initial current density**
138 Despite an important number of cells studied, we observed a large variability of the TREK-1
139 current activation by PUFAs illustrated in **Fig 2A**. The severity of the inclusion criteria (see
140 Material and Methods section) suggests that the variability observed in PUFAs responses is
141 inherent to TREK-1 channel.
142
143 **Fig 2A** illustrates the large variability of PUFA effects based on the fold-increase analysis
144 (I_{PUFA}/I_0).We demonstrated that the variability of the I_{PUFA}/I_0 parameter resulted from the
145 variability of the initial current I_0 but not from the current density at steady-state after the

application of the PUFAs (I_{PUFA}) (**Fig 2B**). Indeed, the calculation of the coefficient of variation (CV = $\frac{SD}{Mean}$) confirmed that the dispersion of the I_{PUFA}/I_0 calculation is higher than the dispersion of the I_{PUFA} at steady-state of the activation (**Fig 2C**). Thus, CV modification is in accordance with the hypothesis that the variability of I_0 is responsible of the variability of the I_{PUFA}/I_0 parameter.

To better characterize the relationship between I_0 and I_{PUFA}/I_0, we plotted the fold-increase of TREK-1 current (I_{PUFA}/I_0, Y axis) as a function of the initial current (I_0, X axis). As shown in **Fig 3A,** there is a non-linear relationship between I_{PUFA}/I_0 and I_0. This relationship can be linearized by log-transforming the data (Log10) (**Fig 3B**). Thus, the effects of all PUFAs but C22:5 n-3 depends on I_0, independently of the absolute amplitude of I_{PUFA}. Therefore, there is a negative relationship between Log10(I_{PUFA}/I_0) and Log10(I_0): C18:2 n-6 (R^2=0.82, p-value=0.0001), C20:2 n-6 (R^2=0.66, p-value=0.0271), C20:4 n-3 (R^2=0.80, p-value=0.0001), C20:4 n-6 (R^2=0.50, p-value=0.0023), C20:5 n-3 (R^2=0.53, 0.0008), C22:5 n-6 (R^2=0.84, p-value=0.0001) and C22:6 n-3 (R^2=0.68, p-value=0.0001) (**Fig 3B, Table 2**). To determine if the observed variability is due to the cellular model that we use, or not, we also used two other models: another stable model of TREK-1 overexpression (Andharia *et al*, 2017) and transiently transfected HEK 293T cells with TREK-1 (pIRES2 *KCNK2* WT) (**Figure 3C**). The I_{PUFA}/I_0 variability observed can be explained by the variety of constitutively active TREK-1 channels at resting condition.

Thanks to the linear regression analysis, we obtained the Y-intercept which reflects the fold-activation of TREK-1 current for an unitary current (Log(1)=0). The Y-intercept of DPA n-3 cannot be calculated since there was no correlation between I_{PUFA}/I_0 and I_0. For the 7 others PUFAs, the Y-intercept values allow their separation into 3 groupes with the following activation sequence : C22:6 n-3, C22:5 n-6, C18:2 n-6 > C20:5 n-3, C20:4 n-6 > C20:4 n-3, C20:2 n-6 (**Table 2**). Then, plotting the relationship between Y-intercept (Y axis) and the

171 number of carbons (X axis) reveled once again that there is no correlation between the fold-
172 activation of TREK-1 and the acyl chain length of PUFAs (**Fig 3D**). There is also no
173 correlation with the number of double bounds (**Fig 3E**). In conclusion, TREK-1 activation by
174 PUFAs is definitively not dependent of the acyl chain length and the number of double bond
175 (**Fig 1D-G** and **Fig 3D-E**).
176

177 **Variable activation rate suggests different binding affinities of PUFAs for TREK-1**
178 **channel**

179 To explore a new way of action of PUFAs on TREK-1 channel, we analyzed and compared
180 the kinetics of activation of TREK-1 perfusing PUFAs or ML402, a binding activator of
181 TREK-1. **Fig 4A to C** represent the mean ± SEM of the normalized current densities
182 ($\frac{I-I_0}{I_{PUFA}-I_0}$) over the time in response to PUFA n-6, PUFA n-3 and ML402, respectively.
183 Representative traces of current densities activation are presented on the right panels.
184 Activation kinetics were fitted with a sigmoid equation (see material and method
185 **equation(3)**) and the activation rate (min^{-1}) was calculated as the inverse of the slope of the
186 sigmoid (**Fig 4D**). We were able to distinguish at least two types of activation rate, a fast one
187 above 3 min^{-1} (C18:2 n-6, C22:6 n-3 and ML402) and a slow one less than 3 min^{-1} (C20:2 n-
188 6, C20:4 n-3, C20:4 n-6, C20:5 n-3, C22:5 n-6 and C22:5 n-3). As reported in **Table 3**, the
189 averaged half-activation of TREK-1 channel was smaller for C18:2 n-6 and C22:6 n-3, both
190 having comparable kinetics to those observed for ML402. Although there were no significant
191 differences between these three compounds and C22:5 n-6 and C20:5 n-3, the kinetics of the
192 latters appeared slightly slower (**Fig 4D, Table 3**). In contrast, C20:4 n-3, C20:4 n-6 and
193 C22:5 n-3 had slower kinetics with an averaged half-activation close to 4 min (**Table 3**).
194 Since C18:2 n-6 and C22:6 n-3 have the same fast activation rates and C22:5 n-3 has the
195 slowest one, we assumed that the activation rate of the TREK-1 by PUFAs does not depend

196 on the acyl chain length. However, among the PUFAs, there is a positive correlation between
197 the activation rate (min^{-1}) and the fold-increase of TREK-1 current (I_{PUFA}/I_0) (Spearman
198 correlation test : p-value = 0.007 and r = 0.88; **Fig 4E**). As the stronger activators are the
199 faster activators of TREK-1, we proposed that some PUFAs, as C18:2 n-6 and C22:6 n-3 have
200 a higher binding affinity for TREK-1 which would allow them to activate it faster and
201 stronger.
202
203 **Activation of TREK-1 channel by PUFAs is fully reversible.**
204 To see if the activation of TREK-1 channel by PUFA is due to an insertion and thus a
205 modification of membrane tension, we looked at the washout kinetic with extracellular
206 medium free of Bovin Serum Albumin (BSA). We focused on C18:2 n-6, C20:5 n-3 and
207 C22:6 n-3, the most potent activators of C18, C20 and C22 PUFAs, respectively (**Table 1**).
208 ML402 activation reversed immediately and 50% of washout occurred in less than 1 min (**Fig**
209 **5A and 5B**). C20:5 n-3, had a kinetic of washing (washout 50%: 0.9 ± 0.1 min) comparable to
210 ML402 (**Fig 5A and 5B**). Even though the washout of C18:2 n-6 and C22:6 n-3 was slower
211 than ML402 (washout 50%, mean ± SEM: 2.4 ± 0.2 min, 3.7 ± 0.3 min and 0.4 ± 0.04 min,
212 respectively) , PUFAs effect were also fully reversed under washing. Once again, there is no
213 correlation between the acyl chain length (**Fig 5C**, Spearman correlation tes: p-value > 0.99)
214 or the number of double bounds (**Fig 5D**, Spearman correlation test: p-value > 0.99) and the
215 time needed to reverse TREK-1 activation. C18:2 n-6 and C22:6 n-3, that activated TREK-1
216 at least twice more than ML402 (I/I_0: 24.8 ± 3.3, 29.8 ± 4.4 and 9.6 ± 0.9, respectively), had a
217 total reversibility in few minutes. At this point, we cannot exclude a membrane insertion of
218 PUFAs, but we assume that the main effects of PUFAs on TREK-1 activation could be a
219 direct and reversible interaction of PUFAs with the channel, as ML402, or as it is well known
220 for KCNQ1 (Liin *et al*, 2015) and the Shaker H4 Kv channel (Börjesson *et al*, 2008)

221

222 **Alteration of membrane curvature or fluidity did not explain activation of TREK-1**
223 **channel by PUFAs.**

224 In order to evaluate the membrane curvature and tension effects on the PUFAs-induced
225 TREK-1 activation, we performed experiments in the inside-out configuration of the patch-
226 clamp technique (+30 mV, symmetrical condition: 145 mM KCl). In this configuration, we
227 were able to superfuse molecules at the inner face of the membrane and PUFAs must induce a
228 curvature of the membrane opposite to the one obtained in the whole-cell configuration. As
229 shown in **Figure 6A**, ML402 superfusion at the inner face of the membrane induced a
230 reversible increase of TREK-1 current (**Table 4**). Kinetics of activation and washout were
231 comparable to those obtained in the whole-cell configuration (**Fig 4** and **Fig 5**) suggesting that
232 the ML402-binding site is accessible from the outer and the inner leaflet of the membrane.
233 Interestingly, a comparable reversible activation of TREK-1 channel was obtained for C18:2
234 n-6 and C22:6 n-3 5 µM, suggesting that the membrane curvature is not involved in the
235 activation of TREK-1 channel by PUFAs (**Fig 6B** and **6C, Table 4**).

236 Then, we assessed the membrane fluidity changes during PUFAs application with a
237 pyrenedecanoic acid probe (PDA), analog to lipids. By measuring the ratio of PDA
238 monomer to excimer fluorescence (405nm/470nm ratio), a quantitative assesment of the
239 membrane fluidity can be obtained at different time points by following the ratio modification
240 over time (F/F_0-1). We focus our experiments on C18:2 n-6 and C22:6 n-3 which are the
241 stronger activators of TREK-1 and C18:3 n-3 that failed to activate TREK-1. These 3 PUFAs
242 at 10 µM did not modify the membrane fluidity even after 50 minutes of application, while at
243 100 µM they induced a decreased of F/F_0-1 from T_0 and compared to the control condition
244 (basic extracellular medium). These results indicate that membrane fluidity is not modified by
245 PUFAs at 10 µM (**Fig 7A-C**), at least within 50 minutes of application. In addition, given that

246 TREK-1 activation starts at 1 minute of perfusion of C18:2 n-6 and C22:6 n-3 10 μM (**Fig 4**)
247 it is unlikely that PUFA effects on TREK-1 activation are due to an increase in membrane
248 fluidity. Altogether, these data suggest that at least both C18:2 n-6 and C22:6 n-3 PUFAs
249 activate TREK-1 channel by direct interaction with TREK-1 protein and not by a modification
250 of the membrane fluidity.
251

252 **DHA interacts directly with TREK-1 channel protein in TREK-1 enriched microsomes**

253 In order to assess a potential direct PUFA-TREK-1 interaction, we purified microsomes from
254 hTREK-1/ HEK and native HEK 293T cells and labeled lysine residues of the total proteins to
255 perform affinity measurements using Spectral Shift (SpS). At first glance, we observed
256 similar affinity from C22:6 n-3 in these two type of microsomes : $K_{d,TREK-1}$ ~ 50 μM and
257 $K_{d,HEK}$ ~ 100 μM highlighting a similar mode of association of C22:6 n-3 within the
258 microsomes. However, the SpS signal displayed subtle differences according to whether or
259 not microsomes were enriched in TREK-1 protein. Knowing SpS signal rises from
260 fluorescence recorded by two individual channel, and having a strong reproducibility from
261 each condition, we can derive the following assumption:

262 **(1)** $I_\lambda(\mathrm{TREK1, HEK}) = I_\lambda(\mathrm{TREK1}) + I_\lambda(\mathrm{HEK})$
263
264 Where for each individual wavelength (λ), the fluorescence recorded for the TREK-1-
265 enriched microscomes correspond to both the fluorescence from the labelled empty
266 microsomes and from the labelled TREK-1.
267 Being able to isolate the specific fluorescence associated to TREK-1 ($I_\lambda(\mathrm{TREK1})$) within the
268 TREK-1-enriched microsomes ($I_\lambda(\mathrm{TREK1, HEK})$), we can use individual channel for further
269 calculation using **equation 2**, isolating the SpS signal associated only to TREK-1 by
270 normalizing out the background signal coming for the free microsomes.

271 **(2)** $R(\mathrm{TREK1}) = \frac{I_{670}(\mathrm{TREK1,HEK}) - I_{670}(\mathrm{HEK})}{I_{650}(\mathrm{TREK1,HEK}) - I_{650}(\mathrm{HEK})}$

When performing so, the specific TREK-1 dose response to C22:6 n-3 gives a K_d = 44 µM (**Fig 8**). Despite displaying similar affinities, the TREK-1-enriched microsomes shows a statistically better affinity than the microsomes themselves. However, it is worth noticing only a 2-fold increase of affinity, which may highlight a similar binding mode for both interactions. Altogether, this suggests an interaction mediated by the lipid bilayer, such as a membrane insertion followed by interaction with TREK-1 channel.

DISCUSSION

TREK-1 channel activation by PUFAs does not involve mechano-sensitivity but a direct interaction

In this study, we reported that TREK-1 channel is reversibly activated by polyunsaturated fatty acids (PUFAs), as already shown in different studies, each being focused mainly on one PUFA : AA (Patel *et al*, 1998); LA (Danthi *et al*, 2003); DHA (Ma & Lewis, 2020). Our study is the first to compare the effects of different PUFAs having between 18 to 22 carbon atoms and 2 to 6 double bonds on TREK-1 channel. We demonstrate that C22:6 n-3 and C18:2 n-6 are the most potent activators of TREK-1 with an activation as fast as the one of the direct activator ML402 and a fully reversibility.

TREK subfamily of K2P channels that includes TREK-1, TREK-2 and TRAAK, is characterized by a mechano-sensitivity and therefore, channels could feel changes in the membrane curvature induced by PUFAs insertion as for CPZ (Patel et al., 1998). As PUFAs are anionic amphipath compounds, with a hydrophilic carboxyl group and a lipophilic tail, they preferentially insert into the outer leaflet of the membrane which is positively charged (Martinac *et al*, 1990; Sheetz & Singer, 1974). Thus, the longer the lipophilic carbon chain is, the more the PUFAs will be inserted into the membrane, modifying the local membrane elastic properties (curvature and fluidity) (Leifert *et al*, 1999). Also, for a given carbon chain

length, the fluidity increases with the number of double bonds. According to the bilayer-couple hypothesis, PUFA effects on TREK subfamily channels were supposed to be due to a modification of elastic properties of the membrane leading to an increase of the tension transmitted to the channels (Patel *et al*, 1998). The study of the TRAAK channel activation by PUFAs (C18:2 n-6, C20:4 n-6, C20:5 n-3, C22:6 n-3) in the excised patch configuration shows that TRAAK activation is positively correlated with the carbon chain length of PUFAs and the number of double bonds (Fink *et al*, 1998; Patel *et al*, 2001). However, we found no correlation between the acyl chain length, the number of double bonds and the potentiation of I_{TREK-1}. In the opposite, C18:2 n-6 and C22:6 n-3, respectively the shortest and the longest PUFA tested, are the most potent activators of TREK-1 channel. It is worth to note that C18:3 n-3, which differs only by one double bond from C18:2 n-6, failed to activate TREK-1 channel. Also, C22:6 n-3 having the same number of carbons than C22:5 n-3 is more than twice as effective in activating TREK-1. PUFAs having intermediate acyl chain length produce intermediate activation of TREK-1, in the same range as the direct activator ML402, independently of the double bonds number. In that respect, the bilayer-couple hypothesis suggesting an activation of TREK-1 by PUFAs-induced mechanosensitive pathway is not appropriate. Similar results were obtained in the literature on TREK-2 channel study, C20:4 n-6 being less efficient than C22:6 n-3 and C18:2 n-6 (Lesage *et al*, 2000).

To better characterize the mechanism of action of C22:6 n-3 and C18:2 n-6 on TREK-1, we compared their kinetics of activation and reversibility with those of ML402. ML402 is a direct activator of TREK-1, binding within a cryptic pocket behind the selectivity filter that directly stabilize the C-type gate (Lolicato *et al*, 2017). The activation kinetic of TREK-1 by C22:6 n-3, C18:2 n-6 and ML402 are comparable and faster than the other PUFAs. This suggests a possible interaction of C22:6 n-3 and C18:2 n-6 with the channel like the activator ML402 (Lolicato *et al*, 2017) and the inhibitor norfluoxetine (Dong *et al*, 2015). This hypothesis is

323 reinforced by the inside-out experiments where C22:6 n-3, C18:2 n-6 and ML402 were
324 applied on the inner leaflet of the membrane. Although the PUFA insertion must induce
325 opposite curvartures while they insert from the inner (inside-out configuration) or the outer
326 leaflet (whole-cell configuration), they still activate TREK-1 channel. We finally propose that
327 at least C22:6 n-3 and C18:2 n-6, like ML402, interact with the channel on an accessible site
328 from both the inner and the outer leaflet of the cell, and suggesting a binding site accessible
329 via the lipid bilayer. Studies have already hypothesized that arachidonic acid (C20:4 n-6)
330 could act directly by interacting with the channel (Maingret *et al*, 1999, 2000) and others have
331 already shown that free PUFAs can directly interact with ionic channels. Indeed, C22:6 n-3
332 and C18:3 n-6 interact with K_v7.1 (*KCNKQ1*)(Liin *et al*, 2015; Yazdi *et al*, 2021). PUFAs
333 also interact with Shaker H4 Kv channel closed to the voltage-sensor domaine through the
334 negatively charged carboxyl group (Börjesson *et al*, 2010; Börjesson & Elinder, 2011;
335 Börjesson *et al*, 2008). As TREK-1 lacks a canonical voltage-sensor domain, we can
336 hypothesize that there is another lipophilic binding site in TREK-1 interacting with the
337 carboxyl head of PUFAs. This hypothetical PUFA binding site on TREK-1 does not
338 correspond to the binding site of ML402 since its mutation does not prevent activation by
339 C20:4 n-6 (Lolicato et al., 2017). Moreover, since the steady-state of TREK-1 activation by
340 PUFA and ML402 was reached in a range of the minutes, we suggest that the PUFAs binding-
341 sites have a limited access (Maingret *et al*, 2000). It has to be noted that bovine serum
342 albumin (BSA) is not required to get a reversal effect during the washout as it is supposed to
343 be when the effects are due to membrane insertion of the PUFAs (Kang & Leaf, 1994; Leifert
344 *et al*, 1999).
345 Finally, in both whole-cell and inside-out configurations, the washout kinetics of PUFAs were
346 immediate and the initial current recovered in few minutes. Despite a total reversibility of the
347 TREK-1 activation under washout, we cannot definitively exclude a membrane insertion of

348 PUFAs owing to their lipophilic properties. Nevertheless, if PUFAs insert into the membrane,
349 they do not modify the biophysic properties of the membrane (fluidity, curvature, tension) at
350 10 µM over a 50 min periode whereas TREK-1 is fully activated by PUFAs in few minutes.
351 Affinity measurements between PUFAs and TREK-1-enriched microsomes effectively
352 indicates a binding with the lipid bilayer as observed for the empty microsomes. However,
353 once the signal due to PUFA interaction with the bilayer is subtracted from the total signal, a
354 direct binding of PUFAs to TREK-1 is measurable. This specific interaction displays a
355 stronger affinity ($K_{D,TREK-1}$ ~ 44 µM) than the simple signal involving PUFA binding with the
356 bilayer of the microsomes. Therefore, we propose that two mechanisms act together to
357 increase I_{TREK-1}: (1)PUFA insertion into the membrane, with no modification of its elastic
358 properties, is probably recquired to reach (2) a lipophilic binding site on TREK-1 channel
359 accessible via the lipid bilayer as for the Shaker channel (Börjesson & Elinder, 2011)
360

361 **Initial TREK-1 variability influence PUFAs response**

362 An unexpected result of this study is the observation that the PUFA effects depend on the
363 TREK-1 initial current. This variability in initial I_{TREK-1} might have many origins such as
364 different levels of post-translationnal modifications, different channels recruitment into the
365 membrane or even the presence of 2 different conductances of TREK-1 channel at the single
366 channel level (Xian Tao Li *et al*, 2006; Andharia *et al*, 2017). A comparable variability in the
367 current-fold increase induced by PUFAs was already observed for TREK-1 activation by AA
368 (Maingret *et al*, 2000), TRAAK (Fink *et al*, 1998; Patel *et al*, 2001) and TREK-2 (Bang *et al*,
369 2000; Lesage *et al*, 2000) but never explained.
370 It is important to note that all these studies were performed on COS-7 cells or HEK-293 cells
371 where mammalian post-translational modifications exist. In the study of Ma and Lewis in
372 2020, whole-cell recording of TREK-1 and TREK-2 by arachidonic acid were performed in

oocytes (*Xenopus Laevis*) and no such variability in the current fold-increase was observed. It is known that in this heterologous expression model, post-translational modification are different (Mantegazza *et al*, 2010). Therefore, the possibility that constitutive TREK-1 current varies according to the phosphorylation level (or other modifications) and influence the effects of PUFAs should be taken in consideration. It is known that TREK-1 channel is modulated by intracellular pathways, related to PKA, PKC and PKG signalizations (Koh *et al*, 2001; Murbartián *et al*, 2005; Honoré, 2007), but to the best of our knowledge, no study between PUFA activation of TREK-1 and phosphorylation levels has been performed so far. As a consequence of this variability, to study the effect of an activator of I_{TREK-1}, we need a sufficient number of cells to apply the Y-intercept of the regression line, probably the best indicator of the degree of activation of TREK-1. The existence of such variability should be taken into consideration in pathophysiological studies associated with variability of expression or response, potentially demultiplying the heterogeneity of TREK-1 response to activators.

Surprisingly, one of the most efficient activator of TREK-1 channel is C18:2 n-6. As TREK-1 is expressed in cardiomyocytes (Li & Toyoda, 2015; Kelly *et al*, 2006; Decher *et al*, 2017) C18:2 n-6 should modulate action potential shape and resting membrane potential.This suggests that C18:2 n-6 could display potent cardio as well as neuroprotective effects. If anti-arrhythmic properties of omega-3 PUFAs have been thoroughly studied (Kang & Leaf, 1994, 1996; Siscovick *et al*, 2017), the potential anti-arrhythmic effect of omega-6 PUFAs such as C18:2 n-6 has never been considered. C18:2 n-6 can be found in vegetarian and Mediterranean diets, both diets having cardioprotective vertues (de Lorgeril *et al*, 1994; Barnard *et al*, 2019). In both cases the beneficial effects are attributed to the presence of anti-

397 oxidant molecules and C18:3 n-3 but a possible beneficial effect of C18:2 n-6 has never been
398 explored.
399
400 **CONCLUSION**
401 To conclude, there is no relationship between the carbon number of the acyl chain, the
402 number of double bonds and the activation of TREK-1 channel. Its most potent activators are
403 C18:2 n-6 (linoleic acid) and C22:6 n-3 (docosahexaenoic acid) and kinetics analysis suggest
404 a direct interaction of PUFAs on TREK-1 through a lipophilic binding site. This direct
405 activation of PUFAs in TREK-1 could require the membrane insertion of PUFAs to facilitate
406 the access to the binding site in the channel.
407
408 **MATERIEL AND METHODS**
409
410 **Cell culture**
411 We used a HEK-293T cell line for spectral shift mesurement and two HEK/hTREK-1 cell
412 lines that stably overexpress the human TREK-1 channel subunit (Moha ou Maati *et al*, 2011;
413 Andharia *et al*, 2017) for electrophysiological experiments and spectral shift mesurement.
414 Cells were grown in an atmosphere of 95% air/5% CO_2 in Dulbecco's modified Eagle's
415 medium and Glutamax (Invitrogen, Cergy- Pontoise, France) supplemented with 10% (v/v)
416 heat inactivated fetal bovine serum and 0.5 mg/mL G418 to maintain a selection pressure in
417 the HEK/hTREK-1 cell line.
418 The transient expression of TREK-1 was performed in the HEK 293T cell line. The pIRES2
419 plasmid in which the coding sequence of TREK-1 (pIRES2 *KCNK2* WT) was inserted, was
420 transfected in HEK 293T cells using the jetPEI® kit (Ozyme) and following the manufacturer
421 protocol. Briefly, 48h before electrophysiological experiments, cells were transfected with a

422 mix of the water-soluble polymer jetPEI® with DNA at 6 ng/mL and then seeded in 35x10
423 mm dishes (Falcon) in presence of 0.5 mg/mL of G418

424 **Electrophysiology**

425 Currents were recorded from hTREK-1/HEK-cells using the patch-clamp technique in whole-
426 cell recording (WCR) configuration and in inside-out (IO) configuration. Patch pipette having
427 2.5-4 MΩ resistances (WCR) and 5-7 MΩ resistances (IO) were obtained from borosilicate
428 glass capillaries by using a two-stage vertical puller (PC- 10, Narishige, London, UK).
429 Current acquisition was performed with an Axopatch 200B amplifier (Axon Instrument,
430 Sunnyvale, CA, USA) and low-pass filtered at 5 kHz (WCR) and 2 kHz (IO). Data were
431 digitalized with a digidata 1550B (Axon Instrument, Sunnyvale, CA, USA) at 10 kHz. The
432 pClamp10.7 (Axon Instrument) software was used to impose stimulations protocols and
433 record TREK-1 current. In WCR, cells were kept for experiments if the series resistance were
434 lower than 8 MΩ, the membrane capacitance between 20 and 35 pF.

435 The experiments were performed at room temperature (~22 °C). Cells were continuously
436 superfused with a extracellular medium and modulatory compounds at a rate of 1-1.5 mL/min.
437 The dishes volume was kept constant at 2.5-3 mL using a vacuum system, connected to a
438 peristaltic pump (ISMATEC). Using different extracellular potassium concentrations (5 mM
439 KCl or 15 mM KCl), changes in membrane potential were measured in current-clamp
440 allowing to determine the time to change completely the medium around the patched-cells (Le
441 Guennec & Noble, 1994). A complete change of the extracellular medium around the
442 patched-cell occurred in less than 15 seconds.

443 ***Whole-cell recording*** : the extracellular medium consisted of (in mM): 150 NaCl, 5 KCl, 3
444 $MgCl_2$, 1 $CaCl_2$ and 10 HEPES pH adjusted to 7.4 with NaOH. The pipette solution consisted
445 of (in mM): 155 KCl, 3 $MgCl_2$, 5 EGTA and 10 HEPES, pH adjusted to 7.2 with KOH. Cells
446 were clamped at a holding potential of -80 mV and superfused with the extracellular medium

for over 1 min before the initial current (I_0) recording. Cells were hyperpolarized to -100 mV for 50 ms and then the macroscopic outward TREK-1 current was elicited with an 800 ms voltage ramp protocol from -100 mV to +30 mV every ten seconds (see the ramp protocole in **Fig 1A**). Thus, the evolution of the current amplitude changes during compound superfusion was followed in real time (**Fig 1B**). A minimum of 3 min superfusion was applied even when the tested compound showed no effect and the superfusion condition was switched once a steady-state was reached. In the case where the tested compound had no effect, a positive control of the TREK-1 activation was performed with 10 µM docosahexaenoic acid (DHA, C22:6 n-3).

Data analysis (WCR): Once at steady-state, the current amplitude at 0 mV during the voltage ramp was measured from the average of the last 3 sweeps over a delta of 1 mV (-0,5 mV to 0,5 mV) to get out of the noise. Current amplitudes are expressed in current densities (pA/pF) to reduce the variability due to cell size. Activation an washout kinetics were followed at 0 mV. The activation kinetics from each cell of each compound (PUFAs and ML402) was fitted with a sigmoidal equation (**Fig 5**):

$$\textbf{(3)}\ I_t = I_0 + \frac{(I_{PUFA} - I_0)}{1 + e^{\frac{t_{50} - t}{slope}}}$$

where I_0 is the initial current and I_{PUFA} is the current caused by PUFA or ML402 at 10 µM concentration. The activation rate (min^{-1}) was then calculated as : activation rate = $\frac{1}{Slope}$.

Inside-out configuration: bath medium contained (in mM) : 140 NaCl, 4.8 KCl, 1.2 $MgCl_2$, 10 glucose, 10 HEPES, pH adjusted to 7.4 with NaOH. After excising the membrane patch, the bath medium was replaced by the a medium identical to the pipette medium consisted of (mM): 145 KCl, 1.2 $MgCl_2$, 10 glucose, 10 HEPES, pH adjusted to 7.2 with KOH. Cells were clamped at a holding potential of 0 mV, the theorical equilibrium potential for K^+ ions in this

472 condition. Then, the amplitude current was followed at +30 mV in real time during the
473 perfusion of compounds and the washout.
474
475 **Membrane fluidity experiments**
476 Membrane fluidity was assessed using the pyrenedecanoic acid probe (PDA), a probe analog
477 to lipids that incorporates into the cell membrane. The probes in the membrane form
478 monomers and excimers, with a rate of excimer proportional to the membrane fluidity. Under
479 PUFAs (C18:2 n-6, C18:3 n-3, C22:6 n-3) application at 10 µM and 100 µM, we measured
480 the emission spectrum of the PDA: 470 nm for the excimers and 400 nm for the the
481 monomers. The monitoring of the fluorescent ratio 470/400 nm shift over time with PUFAs
482 allowed a quantitative monitoring of the membrane fluidity changes due to PUFAs insertion
483 into the membrane. Briefly, HEK/hTREK-1 cells were grown in culture in glass bottom
484 culture dishes (MatTek, Ashland, U.S.A). Before fluorescent experiment, adherent
485 HEK/hTREK-1 cells were incubated 1h at room temperature in the dark with 5 µM of the
486 fluorescent lipid reagent probe in buffer provided in the membrane fluidity kit (Abcam). After
487 incubation, the unicorporated probes were removed by washing cells twice with the same
488 extracellular medium that used for WCR experiments. Epifluorescence microscopic
489 experiments were performed on a 40X lens using excitation light filter with a 370-mm
490 dichroic filter (Zeiss). Emitted light were taken at 480±15 nm and 405±10 nm and the
491 480/405 nm ratio was calculated at intial time before PUFA application (T_0) and T_2 (2 min),
492 T_4, T_6, T_8, T_{10}, T_{20}, T_{30}, T_{40}, T_{50} and T_{60}. The 470/400 nm ratio was calculated as the average
493 ratio overs 5 s. Then, the 470/400 nm ratio was normalized as (F/F_0)-1 and represented over
494 time (**Fig 7**) with F the ratio of fluorescence corresponding to a time T_t and F_0 the ratio
495 corresponding to the T_0.

496 **Microsomes preparation**

497 Microsomes were obtained from the HEK/hTREK-1 cell line and from the HEK 293T cell
498 line as control. Briefly, cells were cultured in T75 flasks until confluence.Then, cells were
499 washed with PBS twice and centrifugated 5 min at 15,000 RPM. The pellet was lysed in a 20
500 mM PIPES buffer (300 mM Sucrose, 20 mM PIPES, pH 7 with NaOH). Membranes were
501 then mechanically braked up using insulin syringe. Samples were centrifuged 20 min at
502 10,000 g at 4°C. Lysis protocol was repeated twice. The pellet was discarded and the
503 supernatant containing plasma membrane and thus transmembrane proteins was
504 ultracentifugated 1h at 32,000 RPM at 4°C (Optima^{TM}L-90K Ultracentrifuge, Beckamn
505 Coulter; Rotor SW60Ti). The pellet containing microsomes was resuspended in 5 mM PIPES
506 (300 mM Sucrose, 5 mM PIPES, pH 7.4 with NaOH) at a protein concentration adjusted to 25
507 mg/mL and conserved at -20°C 2 days before the spectral shift measurment.

508

509 **Spectral shift measurement**

510 Microsomes of HEK 293T cell lin and HEK/hTREK-1 cell line were used to evaluate the
511 TREK-1-PUFAs interaction with HEK 293T microsomes as control. Briefly, the proteins
512 contained in the microsomes were labeled on the lysine residues with a fluorescent dye
513 (MO_L011 RED-NHS 2nd generation, NanoTemper Tehnologies GmbH) following the
514 manufacturer protocol. The 20 µL at 600 µM of dye were used to labelled 200 µL of
515 microsomes, thus leading to a final incubation volume of 200 + 20 µL. After 20 min of
516 incubation, the 220 µL of labeled microsomes were applied to a gravity size exclusion B-
517 column supplied in the kit, following the manufacturer protocol until etution. Labeled
518 microsomes were eluted with 5 x 200 µL of the 5mM PIPES buffer. 5 fractions of 200 µL
519 were collected in a clean Eppendorf. The first elution fraction contains the labeled
520 microsomes while the last fractions contain more free dye. The fluorescence intensity of

521 fraction 1, 2 and 3 were verified and fractions with a fluorescence count between 400 and
522 2,000, using 100% excitation power, were used for the experiment after a 10 min
523 centrifugation at 16,000 g to avoid homogeneity problem. A serial dilution of C22:6 n-3 over
524 16 points following 1:1 pattern was set up and subsequently mixed with labeled microsomes
525 and loaded into standard capillaries (NanoTemper Technologies GmbH). The total proteins
526 concentration in microsomes was kept around 2,5 µg/mL whereas C22:6 n-3 was titrated from
527 1 mM to 30,5 nM. The read out was performed on a Monolith X instrument from
528 NanoTemper Technologies GmbH. The samples were subjected to SpS and MST
529 measurments and only SpS was analyzed due to the normalization requirments. The changes
530 in the maxima emission wavelength following a ratiometric measurement upon protein-C22:6
531 n-3 complex formation was used to generate a binding curve as a function of C22:6 n-3
532 concentrations (Langer *et al*, 2022). The data were pulled from 9 and 5 individual repeat for
533 the TREK-enriched microsomes and from HEK 293T microsomes respectively. Data
534 processing and analysis were carried out using the MO.Control 3 software from NanoTemper
535 Technologies followed by normalization as described in the results section. All the data points
536 presenting signs of irregularity were automatically discarded upon merging the data, as
537 documented in the software.

538 **Chemicals**

539 In this study we tested one direct activator of TREK-1, ML402, one saturated fatty acid,
540 stearic acid, one monounsaturated fatty acid, oleic acid, 9 different PUFAs having between 18
541 and 22 carbons and 2 to 6 double bonds (**Table 1**). All reagents are summarized in the
542 reagents and tools table. 10 mM stock solutions were prepared by dissolving PUFAs in
543 absolute ethanol, ML402 in DMSO. PUFAs and ML402 were stored at -80 °. 10 µM solutions
544 were obtained by diluting an aliquot of stock solution in the extracellular medium just before

545 use for WCR experiments. Cells for current recordings were first superfused with
546 extracellular medium containing ethanol at 1/1000 as a control.
547
548
549

Reagent/resource	Source	Identifier or catalog number
Experimental model		
HEK hTREK-1 cell line	(Moha ou Maati *et al*, 2011)	
HEK 293T/hTREK-1 cell line	(Andharia *et al*, 2017)	
HEK-293 T cell line		
Cell culture		
DMEM + Glutamax	ThermoFisher	31966-021
Fetal bovine serum	Sigma-Aldrich	F7524-500ML
jetPEI®	Ozyme	POL101000053
Trypsin-EDTA	ThermoFisher	25300-054
G418 (geneticin)	Sigma-Aldrich	4727878001
Chemicals		
Linoleic acid	Sigma-Aldrich	L1376-500MG
cis-11,14-Eicosadienoic acid	Sigma-Aldrich	E3127-25MG
Oleic acid	Sigma-Aldrich	O1008
Stearic acid	Sigma-Aldrich	S4751-1G
Cis-5,8,11,14,17-Eicosapentaenoic acid	Sigma-Aldrich	E2011-10MG
Cis-4,7,10,13,16,19-Docosahexaenoic acid	Sigma-Aldrich	D2534-100MG
Alpha-linolenic acid	Sigma-Aldrich	L-039-1ML
Docosapentaenoic acid (cis-7,10,13,16,19)	Sigma-Aldrich	D-120-1ML
Cis-4,7,10,13,16-Docosapentaenoic acid	Sigma-Aldrich	18566-10MG
Arachidonic acid	Sigma-Aldrich	A36-11-100MG
Omega-3 Arachidonic acid	Santa Cruz	sc229695
ML402	MedChemExpress	HY-104027
NanoTemper experiment		

Protein labeling kit	NanoTemper	MO-L011
Capillaries	NanoTemper	MO-K022
Monolith™ X instrument	NanoTemper	
Membrane fluidity experiment		
Membrane fluidity kit	Abcam	ab189819
Glass Bottom culture dishes	MatTek	P35G-0-14-C

Statistical analysis

All set of experiments were performed on at least three different batches (congelation and/or passage) of cells. All descriptive statistics are displayed from **Table 1** to **Table 4**. Statistical analysis were performed using Prism software (GraphPad Prism 9, Inc., USA). Spearman correlation test were performed and the p-value indicates the significance of the correlation and the r parameter indicates the direction of the correlation (negative or positive). For the linear regression, the p-value indicates the significance of the relationship, the R^2 indicates the goodness of the fit an the error bars represent the 90 % confidence interval. Kruskal-Wallis test followed by a *post hoc* Dunn's test was used for multiple comparison of unmatched data. A p-value of 0.05 or less was considered as statistically significant. The differences between more than 2 groups are displayed by the letter code, where groups that do not share the same letter are significantly different.

564 **AUTHORS CONTRIBUTION**

565 EB carried out the experiments (WCR and IO), set up experiments and protocols, conceived
566 the original idea and wrote the manuscript.
567 EA carried out the experiments (WCR) and discussed the results.
568 JB carried out the experiments (WCR) and discussed the results.
569 JL carried out the experiments(WCR) and discussed the results.
570 XB carried out the experiments (IO) and discussed the results.
571 AE participated to the PUFAs structure discussion.
572 CV helped supervise the project on chemistry of PUFAs and discussed the results.
573 PS helped in the design and result analyses of affinity tests.
574 TD helped supervise the project on chemistry of PUFAs and discussed the results.
575 JMG helped supervise the project on chemistry of PUFAs and discussed the results.
576 CO helped supervise the project on chemistry of PUFAs and discussed the results.
577 JYL set up experiments and protocols, conceived the original idea, wrote the manuscript and
578 supervised the project.
579 HMM provided HEK hTREK-1 cells
580 MD set up experiments and protocols, conceived the original idea, wrote the manuscript and
581 supervised the project.
582

583 **ACKNOWLEDGEMENT**

584 This work is supported by the Agence Nationale de la Recherche : acronym TA-BOOm
585 (ANR-20-CE44-0001), Région Occitanie Pyrénées-Méditerranée (MNE-AGPI03), Key
586 Initiative Montpellier Université d'Excellence (KIM Biomarkers and Therapies) and the CBS2
587 doctoral school. We thank Pr OKADA for the kind gift TR-1 cells: a 293 T cell line that
588 stably expresses TREK-1 channel.

589

590

591

592

REFERENCES

Andharia N, Joseph A, Hayashi M, Okada M & Matsuda H (2017) Involvement of intracellular transport in TREK-1c current run-up in 293T cells. *Channels Austin Tex* 11: 224–235

Bang H, Kim Y & Kim D (2000) TREK-2, a new member of the mechanosensitive tandem-pore K+ channel family. *J Biol Chem* 275: 17412–17419

Barnard ND, Goldman DM, Loomis JF, Kahleova H, Levin SM, Neabore S & Batts TC (2019) Plant-Based Diets for Cardiovascular Safety and Performance in Endurance Sports. *Nutrients* 11: E130

Bechard E, Bride J, Le Guennec J-Y, Brette F & Demion M (2022) TREK-1 in the heart: Potential physiological and pathophysiological roles. *Front Physiol* 13: 1095102

Börjesson SI & Elinder F (2011) An electrostatic potassium channel opener targeting the final voltage sensor transition. *J Gen Physiol* 137: 563–577

Börjesson SI, Hammarström S & Elinder F (2008) Lipoelectric modification of ion channel voltage gating by polyunsaturated fatty acids. *Biophys J* 95: 2242–2253

Börjesson SI, Parkkari T, Hammarström S & Elinder F (2010) Electrostatic tuning of cellular excitability. *Biophys J* 98: 396–403

Danthi S, Enyeart JA & Enyeart JJ (2003) Modulation of native TREK-1 and Kv1.4 K+ channels by polyunsaturated fatty acids and lysophospholipids. *J Membr Biol* 195: 147–164

Decher N, Ortiz-Bonnin B, Friedrich C, Schewe M, Kiper AK, Rinné S, Seemann G, Peyronnet R, Zumhagen S, Bustos D, *et al* (2017) Sodium permeable and 'hypersensitive' TREK-1 channels cause ventricular tachycardia. *EMBO Mol Med* 9: 403–414

Djillani A, Mazella J, Heurteaux C & Borsotto M (2019) Role of TREK-1 in Health and Disease, Focus on the Central Nervous System. *Front Pharmacol* 10: 379

Dong YY, Pike ACW, Mackenzie A, McClenaghan C, Aryal P, Dong L, Quigley A, Grieben M, Goubin S, Mukhopadhyay S, *et al* (2015) K2P channel gating mechanisms revealed by structures of TREK-2 and a complex with Prozac. *Science* 347: 1256–1259

Fink M, Duprat F, Lesage F, Reyes R, Romey G, Heurteaux C & Lazdunski M (1996) Cloning, functional expression and brain localization of a novel unconventional outward rectifier K+ channel. *EMBO J* 15: 6854–6862

Fink M, Lesage F, Duprat F, Heurteaux C, Reyes R, Fosset M & Lazdunski M (1998) A neuronal two P domain K+ channel stimulated by arachidonic acid and polyunsaturated fatty acids. *EMBO J* 17: 3297–3308

Heurteaux C, Guy N, Laigle C, Blondeau N, Duprat F, Mazzuca M, Lang-Lazdunski L, Widmann C, Zanzouri M, Romey G, *et al* (2004) TREK-1, a K+ channel involved in neuroprotection and general anesthesia. *EMBO J* 23: 2684–2695

Honoré E (2007) The neuronal background K2P channels: focus on TREK1. *Nat Rev Neurosci* 8: 251–261

Kamatham S, Waters CM, Schwingshackl A & Mancarella S (2019) TREK-1 protects the heart against ischemia-reperfusion-induced injury and from adverse remodeling after myocardial infarction. *Pflugers Arch* 471: 1263–1272

Kang JX & Leaf A (1994) Effects of long-chain polyunsaturated fatty acids on the contraction of neonatal rat cardiac myocytes. *Proc Natl Acad Sci U S A* 91: 9886–9890

Kang JX & Leaf A (1996) Evidence that free polyunsaturated fatty acids modify Na+ channels by directly binding to the channel proteins. *Proc Natl Acad Sci U S A* 93: 3542–3546

Kelly D, Mackenzie L, Hunter P, Smaill B & Saint DA (2006) Gene expression of stretch-activated channels and mechanoelectric feedback in the heart. *Clin Exp Pharmacol Physiol* 33: 642–648

Koh SD, Monaghan K, Sergeant GP, Ro S, Walker RL, Sanders KM & Horowitz B (2001) TREK-1 regulation by nitric oxide and cGMP-dependent protein kinase. An essential role in smooth muscle inhibitory neurotransmission. *J Biol Chem* 276: 44338–44346

Lamas JA & Fernández-Fernández D (2019) Tandem pore TWIK-related potassium channels and neuroprotection. *Neural Regen Res* 14: 1293–1308

Langer A, Lüdecke A, Bartoschik T, Cehlar O, Duhr S, Baaske P & Streicher W (2022) A New Spectral Shift-Based Method to Characterize Molecular Interactions. *ASSAY Drug Dev Technol* 20: 83–94

Le Guennec JV & Noble D (1994) Effects of rapid changes of external Na+ concentration at different moments during the action potential in guinea-pig myocytes. *J Physiol* 478 Pt 3: 493–504

Leifert WR, McMurchie EJ & Saint DA (1999) Inhibition of cardiac sodium currents in adult rat myocytes by n-3 polyunsaturated fatty acids. *J Physiol* 520 Pt 3: 671–679

Lesage F, Terrenoire C, Romey G & Lazdunski M (2000) Human TREK2, a 2P domain mechano-sensitive K+ channel with multiple regulations by polyunsaturated fatty acids, lysophospholipids, and Gs, Gi, and Gq protein-coupled receptors. *J Biol Chem* 275: 28398–28405

Li X-Y & Toyoda H (2015) Role of leak potassium channels in pain signaling. *Brain Res Bull* 119: 73–79

Liin SI, Silverå Ejneby M, Barro-Soria R, Skarsfeldt MA, Larsson JE, Starck Härlin F, Parkkari T, Bentzen BH, Schmitt N, Larsson HP, *et al* (2015) Polyunsaturated fatty acid analogs act antiarrhythmically on the cardiac IKs channel. *Proc Natl Acad Sci U S A* 112: 5714–5719

Lolicato M, Arrigoni C, Mori T, Sekioka Y, Bryant C, Clark KA & Minor DL (2017) K2P2.1 (TREK-1)-activator complexes reveal a cryptic selectivity filter binding site. *Nature* 547: 364–368

de Lorgeril M, Renaud S, Mamelle N, Salen P, Martin JL, Monjaud I, Guidollet J, Touboul P & Delaye J (1994) Mediterranean alpha-linolenic acid-rich diet in secondary prevention of coronary heart disease. *Lancet Lond Engl* 343: 1454–1459

Ma R & Lewis A (2020) Spadin Selectively Antagonizes Arachidonic Acid Activation of TREK-1 Channels. *Front Pharmacol* 11: 434

Maingret F, Fosset M, Lesage F, Lazdunski M & Honoré E (1999) TRAAK is a mammalian neuronal mechano-gated K+ channel. *J Biol Chem* 274: 1381–1387

Maingret F, Patel AJ, Lesage F, Lazdunski M & Honoré E (2000) Lysophospholipids open the two-pore domain mechano-gated K(+) channels TREK-1 and TRAAK. *J Biol Chem* 275: 10128–10133

Mantegazza M, Rusconi R, Scalmani P, Avanzini G & Franceschetti S (2010) Epileptogenic ion channel mutations: from bedside to bench and, hopefully, back again. *Epilepsy Res* 92: 1–29

Martinac B, Zhu H, Kubalski A, Zhou XL, Culbertson M, Bussey H & Kung C (1990) Yeast K1 killer toxin forms ion channels in sensitive yeast spheroplasts and in artificial liposomes. *Proc Natl Acad Sci U S A* 87: 6228–6232

Moha ou Maati H, Peyronnet R, Devader C, Veyssiere J, Labbal F, Gandin C, Mazella J, Heurteaux C & Borsotto M (2011) A human TREK-1/HEK cell line: a highly efficient screening tool for drug development in neurological diseases. *PloS One* 6: e25602

Murbartián J, Lei Q, Sando JJ & Bayliss DA (2005) Sequential phosphorylation mediates receptor- and kinase-induced inhibition of TREK-1 background potassium channels. *J Biol Chem* 280: 30175–30184

Patel AJ, Honoré E, Maingret F, Lesage F, Fink M, Duprat F & Lazdunski M (1998) A mammalian two pore domain mechano-gated S-like K+ channel. *EMBO J* 17: 4283–4290

Patel AJ, Lazdunski M & Honoré E (2001) Lipid and mechano-gated 2P domain K(+) channels. *Curr Opin Cell Biol* 13: 422–428

Sheetz MP & Singer SJ (1974) Biological membranes as bilayer couples. A molecular mechanism of drug-erythrocyte interactions. *Proc Natl Acad Sci U S A* 71: 4457–4461

Siscovick DS, Barringer TA, Fretts AM, Wu JHY, Lichtenstein AH, Costello RB, Kris-Etherton PM, Jacobson TA, Engler MB, Alger HM, *et al* (2017) Omega-3 Polyunsaturated Fatty Acid (Fish Oil) Supplementation and the Prevention of Clinical Cardiovascular Disease: A Science Advisory From the American Heart Association. *Circulation* 135: e867–e884

Wiedmann F, Rinné S, Donner B, Decher N, Katus HA & Schmidt C (2021) Mechanosensitive TREK-1 two-pore-domain potassium (K2P) channels in the cardiovascular system. *Prog Biophys Mol Biol* 159: 126–135

Xian Tao Li null, Dyachenko V, Zuzarte M, Putzke C, Preisig-Müller R, Isenberg G & Daut J (2006) The stretch-activated potassium channel TREK-1 in rat cardiac ventricular muscle. *Cardiovasc Res* 69: 86–97

Yazdi S, Nikesjö J, Miranda W, Corradi V, Tieleman DP, Noskov SY, Larsson HP & Liin SI (2021) Identification of PUFA interaction sites on the cardiac potassium channel KCNQ1. *J Gen Physiol* 153: e202012850

FIGURE LEGENDS

Figure 1: Activation of TREK-1 channel by PolyUnsaturated Fatty Acids.
A. Illustration of the voltage ramp protocol to record I_{TREK-1} between -100 mV and +30 mV. **B.** A representative traces of current recordings during C22:6 n-3 (DHA) application is shown in one trace *per* 10s (middle). The inset on the right shows the characteristic outward rectifying initial current of TREK-1 (I_0: initial current density). **C.** Effect of 10µM of Norfluoxetine (NrFlx on I_0. **D.** Bar graph showing the initial membrane potential Em_0 (mV) for HEK 293T and HEK hTREK-1 cell lines and the membrane potential Em_{PUFA} of HEK hTREK-1 cells after the PUFA perfusion. **E.** Lack of correlation between the acyl chain length and I/I_0 and **F.** the current density (pA/pF), in response to 10 µM PUFAs at 0 mV. **G.** Lack of correlation between the number of double bounds and I/I_0 and **H.** the current density (pA/pF), in response to 10 µM PUFAs at 0 mV. (Purple: C18:2 n-6, blue: C18:3 n-3, light green : C20:2 n-6, brown: C20:4 n-3, red : C20:4 n-6, green: C20:5 n-3, light green : C22:5 n-3, pink: C22:5 n-6, orange: C22:6 n-3).

Figure 2: Variability of TREK-1 activation by PUFAs
A. Boxplot of the fold increase (I_{PUFA}/I_0) of TREK-1 and **B**. the current density at steady-state (I_{PUFA}, pA/pF) at 0 mV for each PUFA at 10 µM. Boxplots represent the median (lines) with max and min values (error bars). Groups were compared with a Kruskal-Wallis test followed with the *post-hoc* Dunn's test. Two bars having the same letter are not significantly different. **C.** Changes in the coefficient of variation (SD/mean) between I_{PUFA}/I_0 and I_{PUFA} at 0 n(: coefficient of variation for I_{PUFA}/I_0; : coefficient of variation for I_{PUFA}). Both coefficient of variation are superimposed.

Figure 3: Variability in TREK-1 activation by PUFAs depends on the initial current I_0.
A. Scatter plot representations of I_{PUFA}/I_0 as a function of I_0. **B.** Linearization of the I_{PUFA}/I_0 *vs* I_0 relationship following log-transformation for each PUFA. The simple linear regression~~s (~~

742) are represented with the 90% confidence interval (IC; dotted line·····) used to discard one of
743 the C20:4 n-3 and C20:4 n-6 data points (⊠). A point is discarded only if it is out by more than
744 twice the 90% IC. **C.** Relationship between Log10($I_{C22:6\ n\text{-}3}/I_0$) and Log10($I_0$) at 0 mV in
745 different cell lines: HEK hTREK-1 stable cell line #1 (orange), HEK hTREK-1 stable cell line
746 #2 (red) and HEK 293T cells transiently transfected with TREK-1 channel (pIRES2 KCNK2
747 WT 6 ng/µL)(purple). **D.** Lack of correlation between the Y-intercept of the linear
748 regressions obtained before and the acyl chain length, **E.** and the number of double bounds,
749 for each PUFA at 10 µM.
750
751 **Figure 4: Activation kinetics of TREK-1 channel by PUFAs.**
752 **A-C.** Time course showing the effects of 10 µM PUFAs and ML402 on $I_{TREK\text{-}1}$ at 0 mV.
753 PUFAs and ML402 were superfused until the steady-state was reached. *Insets* show the
754 representative current densities recorded in control medium and then under PUFAs or ML402
755 application. **D.** Bar graphs of the activation rate + SEM to reach the steady-state of I_{PUFA}.
756 Groups were compared with a Kruskal-Wallis test followed with the *post-hoc* Dunn's test.
757 Two bars having the same letter are not significantly different. **E.** Relationship between the
758 fold-increase of TREK-1 (I_{PUFA}/I_0) and the activation rate (min^{-1}) (R^2=0.60; p-value=0.02;
759 error barres show the SEM of the I_{PUFA}/I_0 and the activation rate).
760
761 **Figure 5: Washout kinetics of LA, EPA, DHA and ML402.**
762 **A.** Representative traces of the reversibility of the current density with one trace per minute
763 (grey: initial current I_0; colors: PUFA-activated current density at steady-state; black: washout
764 current density). **B.** Normalized current-time curve of the reversibility for each compound
765 (mean ± SEM) with 1 point every 10s. The current was normalized as $(I\text{-}I_0)/(I_{PUFA}\text{-}I_0)$. The
766 inset shows the time to reach 50% of the reversibility of TREK-1 activation. **C.** Lack of
767 correlation between the time for 50 % of washout and the acyl chain length and **D.** the number
768 of double bounds.
769
770 **Figure 6: PUFAs activate TREK-1 in inside-out configuration of patch-clamp.**
771 **A-C.** Representative traces showing the activation and reversibility in inside-out configuration
772 of patch-clamp technique for **A.** ML402 10 µM **B.** C18:2 n-6 5 µM and **C.** C22:6 n-3 5 µM
773 superfused at the inner face of the membrane. Membrane potential was held at +30 mV. The
774 expanded current traces where extracted at the time indicated by the arrows.
775
776 **Figure 7: Membrane fluidity is not altered by PUFAs at 10 µM**
777 **A-C.** Membrane fluidity is not changed over time by 10 µM of PUFA but 100 µM :**A.** C18:3
778 n-3 (10 µM: n=3; 100 µM n=6; CTL n=4), **B.** 18:2 n-6 (10 µM: n=6; 100 µM: n=7; CTL
779 n=6), **C.** C22 :6 n-3 (10 µM: n=5; 100 µM: n=5; CTL n=5),
780
781 **Figure 8** : **Effect C22:6 n-3 on SpS signal in TREK-1-enriched microsomes and non-**
782 **enriched microsomes**
783 (I_λ(TREK1, HEK) represents the binding affinity of C22:6 n-3 (from 1 mM to 30.5 nM) for
784 TREK-1-enriched microsomes from 1 mM to 30.5 nM (n=5-9 experiments).
785
786
787
788
789
790
791

TABLES

806
807

	IUPAC Name		Tail length	Unsaturation number	ω	I_{PUFA}/I_0	I_{PUFA} (pA/pF)
C18:0	Stearic acid	18:0	18	0		1,0 ± 0,1	18.4 ± 5.5
C18:1 n-9	Oleic acid (9)	18:1 Δ 9	18	1	ω-9	7.4 ± 1.9	113,1 ± 24.6
C18:2 n-6	Linoleic acid (9,12)	18:2 Δ 9,12	18	2	ω-6	24.8 ± 3.3	353.7 ± 22.4
C18:3 n-3	α-Linolenic acid (9,12,15)	18:3 Δ 9,12,15	18	3	ω-3	1.4 ± 0.1	20.72 ± 4.2
C20:2 n-6	Eicosadienoic acid (11,14)	20:2 Δ 11,14	20	2	ω-6	10.1 ± 1.2	166.1 ± 16.2
C20:4 n-3	Eicosatetraenoic acid (8,11,14,17)	20:4 Δ 8,11,14,17	20	4	ω-3	10.9 ± 2.0	119.2 ± 15.5
C20:4 n-6	Eicosatetraenoic acid (5,8,11,14)	20:4 Δ 5,8,11,14	20	4	ω-6	15.7 ± 2.1	199.5 ± 23.1
C20:5 n-3	Eicosapentaenoic acid (5,8,11,14,17)	20:5 Δ 5,8,11,14,17	20	5	ω-3	17.4 ± 2.8	211.7 ± 21.0
C22:5 n-6	Docosapentaenoic acid (4,7,10,13,16)	22:5 Δ 4,7,10,13,16	22	5	ω-6	26.1 ± 8.3	245.3 ± 21.4
C22:5 n-3	Docosapentaenoic acid (7,10,13,16,19)	22:5 Δ 7,10,13,16,19	22	5	ω-3	13.3 ± 2.9	147.1 ± 26.6
C22:6 n-3	Docosahexaenoic acid (4,7,10,13,16,19)	22:6 Δ 4,7,10,13,16,19	22	6	ω-3	29.8 ± 4.4	276.8 ± 24.5

Table 1: Fatty acids nomenclature, characteristics and effects on the TREK-1 current in whole-cell configuration of patch-clamp. Values of I_{PUFA}/I_0 and I_{PUFA} are expressed as mean ± SEM.

	n	p-value	R^2	Equation	Y-intercept ± SD
C18:2 n-6	20	0.0001	0.82	Y = -0.9378*X + 2.343	2.3 ± 0.1
C20:2 n-6	7	0.027	0.66	Y = -0.5264*X + 1.621	1.6 ± 0.2
C20:4 n-3	12	0.0001	0.80	Y = -0.6305*X + 1.672	1.7 ± 0.1
C20:4 n-6	16	0.002	0.50	Y = -0.8315*X + 2.083	2.1 ± 0.3
C20:5 n-3	17	0.0008	0.53	Y = -0.7172*X + 1.958	1.9 ± 0.2
C22:5 n-6	11	0.0001	0.84	Y = -1.073*X + 2.462	2.5 ± 0.2
C22:5 n-3	12	0.371	0.08	Y = -0.3221*X + 1.378	1.4 ± 0.4
C22:6 n-3	20	0.0001	0.68	Y = -0.7378*X + 2.133	2.1 ± 0.1

Table 2: Parameters of the linear regression Log10 (I_{PUFA}/I_0)=f(Log10(I_0)).
TREK-1 current was recorded in whole-celle configuration of patch-clamp.The p-value indicates the significativity of the relationship, the R^2 indicates the goodness of the fit and the Y-intercept reflects the fold-activation of TREK-1 current for an unitary current as Log(1)=0.

		Half-activation (min)	Steady-state (min)	Activation rate (min^{-1})
	n	Mean ± SEM	Mean ± SEM	Mean ± SEM
C18:2 n-6	20	1.9 ± 0.2	3.7 ± 0.3	4.5 ± 0.7
C20:2 n-6	7	4.6 ± 0.3	7.4 ± 0.3	0.9 ± 0.1
C20:4 n-3	12	4.6 ± 0.2	7.1 ± 0.2	0.9 ± 0.1
C20:4 n-6	16	3.9 ± 0.3	6.7 ± 0.3	1.1 ± 0.1
C20:5 n-3	17	3.2 ± 0.3	5.7 ± 0.3	2.0 ± 0.3
C22:5 n-6	11	3.1 ± 0.3	5.3 ± 0.4	1.5 ± 0.2
C22:5 n-3	12	4.2 ± 0.4	5.9 ± 0.4	0.9 ± 0.1
C22:6 n-3	20	2.3 ± 0.2	4.3 ± 0.3	3.4 ± 0.4
ML402	19	2.1 ± 0.2	3.9 ± 0.3	3.8 ± 0.5

Table 3: Parameters of the activation kinetic of TREK-1 by PUFAs and ML402 in whole-cell configuration of patch-clamp. Values indicate the time (min) needed to reach the half-activation and the steady-state of the activation of TREK-1. The activation rate (min^{-1}) derived from the sigmoidal fit as : $I_t = I_0 + \frac{(I_{PUFA} - I_0)}{1+e^{\frac{t_{50}-t}{slope}}}$ and activation rate = $\frac{1}{slope}$.

			Steady-state (min)	50% of washout (s)
	n	Concentration (µM)	Mean ± SEM	Mean ± SEM
C18:2 n-6	4	5	4.6 ± 0.4	18.3 ± 6.3
C22:6 n-3	6	5	2.9 ± 0.3	18.3 ± 4.2
ML402	6	10	2.6 ± 0.6	15.5 ± 7.6

Table 4: **Descriptive statistics for TREK-1 activation and washout kinetics in inside-out configuration of patch-clamp.** Values indicate the time needed to reach the steady-state (min) and the time to reach 50% of washout (s).

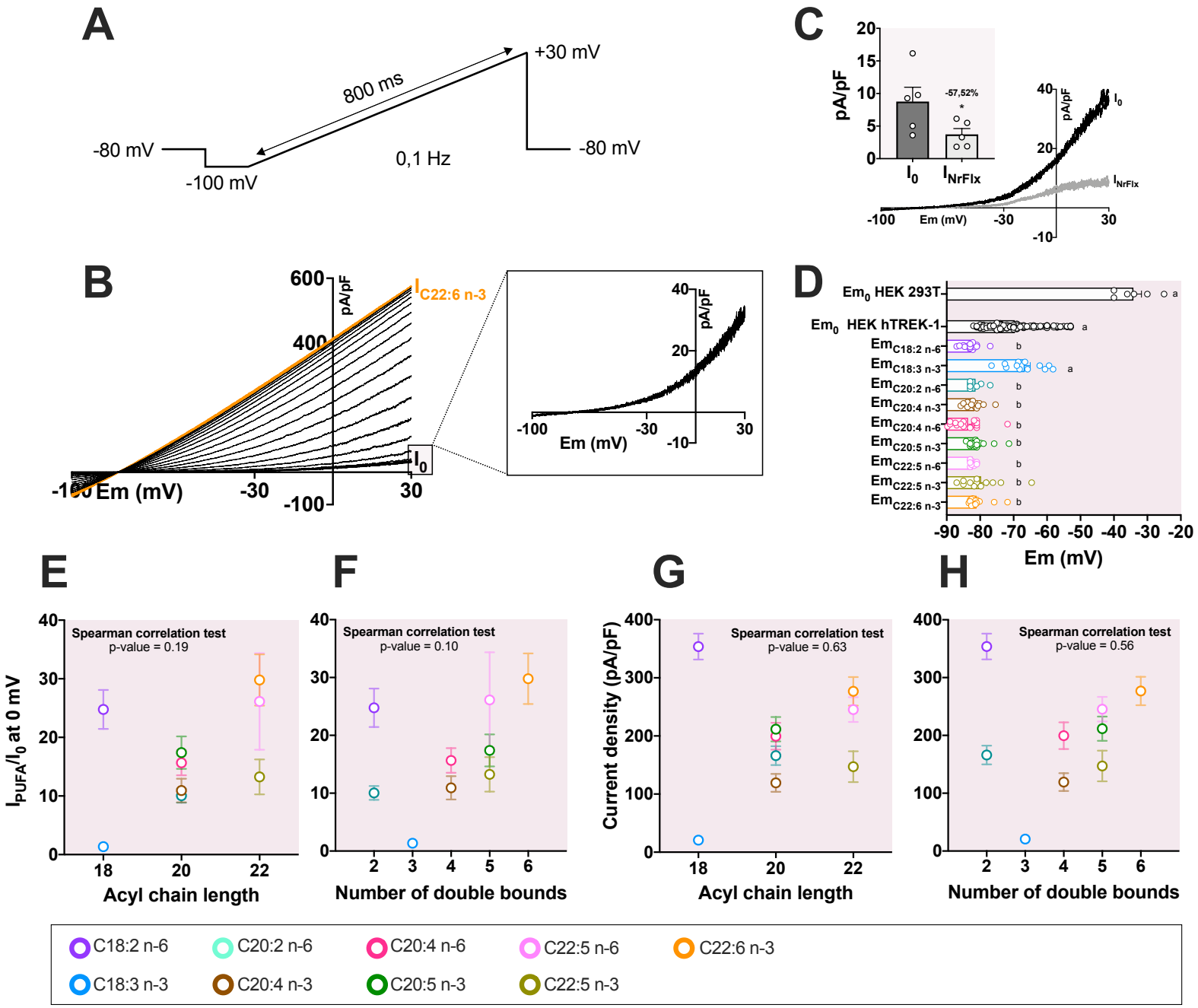
A
+30 mV
800 ms
-80 mV
-100 mV
0,1 Hz
-80 mV
B
600
400
pA/pF
I C22:6 n-3
I0
-100 Em (mV)
-30
30
-100
40
20
pA/pF
-100
-30
30
-10
Em (mV)
C
20
15
10
5
0
pA/pF
-57,52%
*
I0
INrFlx
40
20
pA/pF
I0
INrFlx
-100
Em (mV)
-30
30
-10
D
Em0 HEK 293T
Em0 HEK hTREK-1
EmC18:2 n-6
EmC18:3 n-3
EmC20:2 n-6
EmC20:4 n-3
EmC20:4 n-6
EmC20:5 n-3
EmC22:5 n-6
EmC22:5 n-3
EmC22:6 n-3
a
a
b
a
b
b
b
b
b
b
b
-90 -80 -70 -60 -50 -40 -30 -20
Em (mV)
E
Spearman correlation test
p-value = 0.19
IPUFA/I0 at 0 mV
40
30
20
10
0
18
20
22
Acyl chain length
F
Spearman correlation test
p-value = 0.10
40
30
20
10
0
2
3
4
5
6
Number of double bounds
G
Spearman correlation test
p-value = 0.63
Current density (pA/pF)
400
300
200
100
0
18
20
22
Acyl chain length
H
Spearman correlation test
p-value = 0.56
400
300
200
100
0
2
3
4
5
6
Number of double bounds
C18:2 n-6
C20:2 n-6
C20:4 n-6
C22:5 n-6
C22:6 n-3
C18:3 n-3
C20:4 n-3
C20:5 n-3
C22:5 n-3

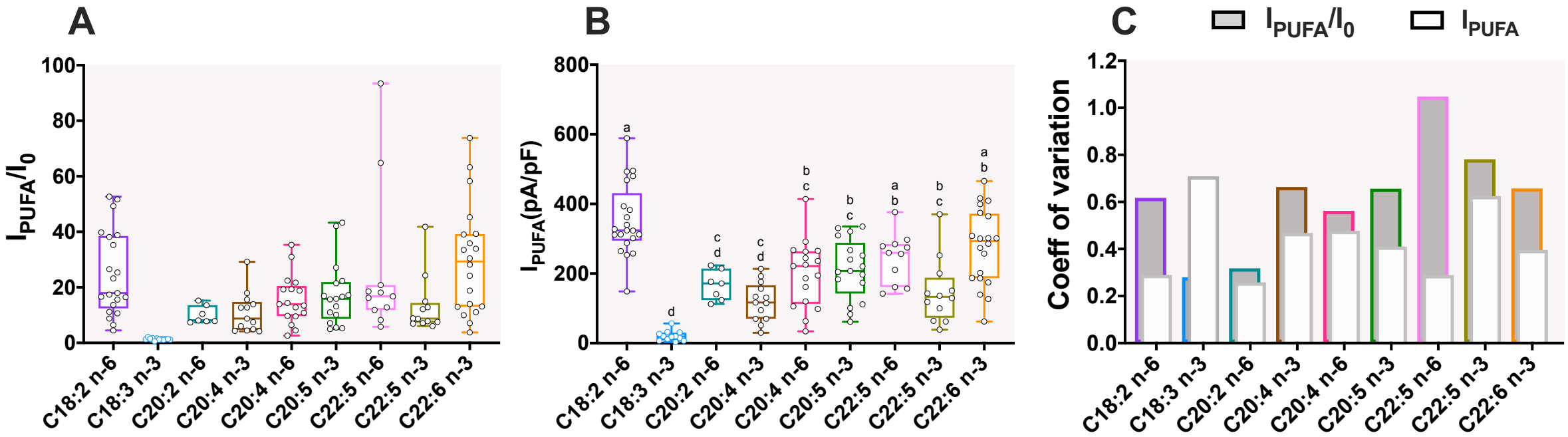
A
B
C
I_{PUFA}/I_0
I_{PUFA}
I_{PUFA}/I_0
I_{PUFA}(pA/pF)
Coeff of variation
C18:2 n-6
C18:3 n-3
C20:2 n-6
C20:4 n-3
C20:4 n-6
C20:5 n-3
C22:5 n-6
C22:5 n-3
C22:6 n-3

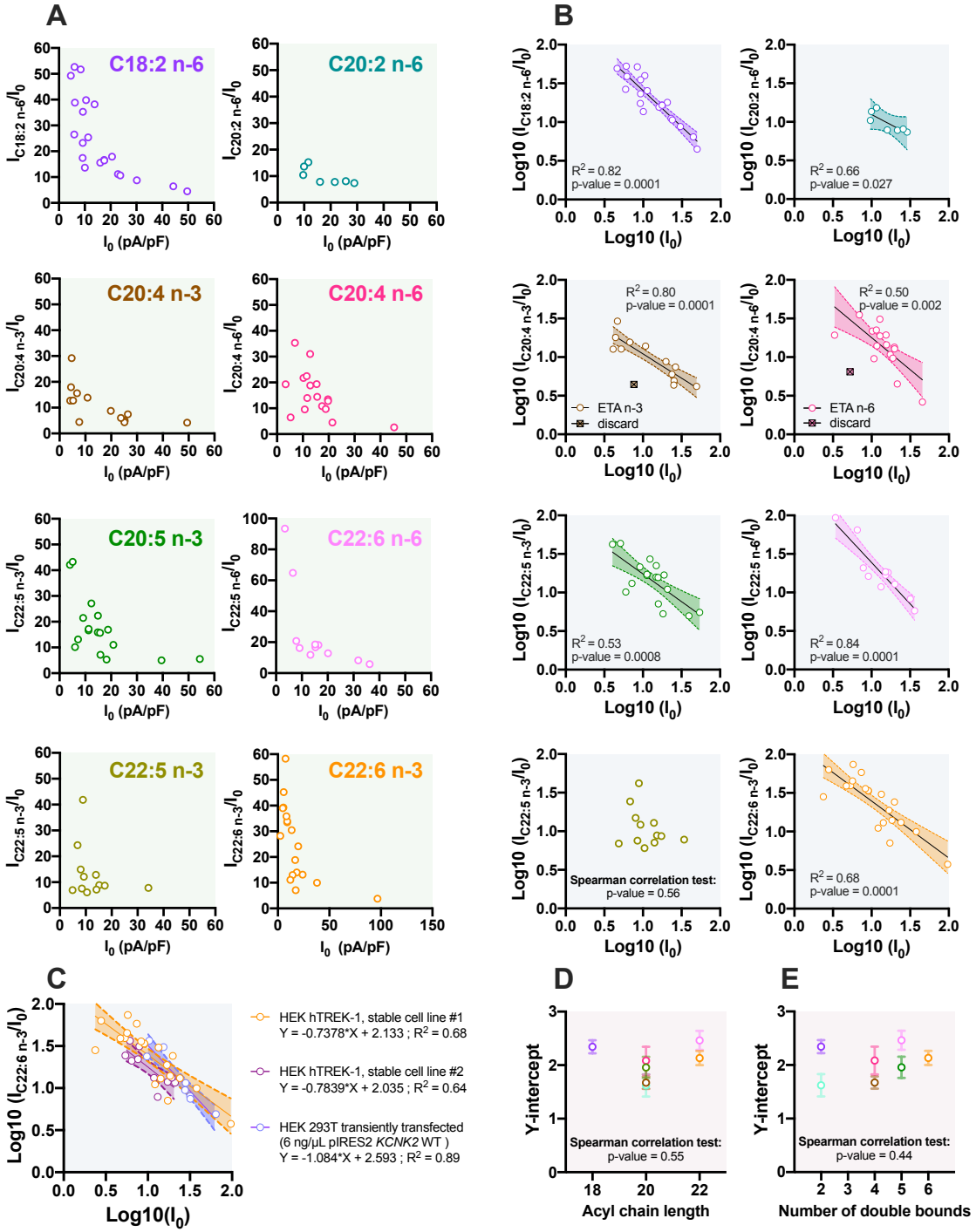
A
C18:2 n-6
C20:2 n-6
C20:4 n-3
C20:4 n-6
C20:5 n-3
C22:6 n-6
C22:5 n-3
C22:6 n-3
I0 (pA/pF)
B
R2 = 0.82
p-value = 0.0001
R2 = 0.66
p-value = 0.027
R2 = 0.80
p-value = 0.0001
ETA n-3
discard
R2 = 0.50
p-value = 0.002
ETA n-6
discard
R2 = 0.53
p-value = 0.0008
R2 = 0.84
p-value = 0.0001
Spearman correlation test:
p-value = 0.56
R2 = 0.68
p-value = 0.0001
Log10 (I0)
C
HEK hTREK-1, stable cell line #1
Y = -0.7378*X + 2.133 ; R2 = 0.68
HEK hTREK-1, stable cell line #2
Y = -0.7839*X + 2.035 ; R2 = 0.64
HEK 293T transiently transfected
(6 ng/µL pIRES2 KCNK2 WT)
Y = -1.084*X + 2.593 ; R2 = 0.89
Log10(I0)
D
Y-intercept
Spearman correlation test:
p-value = 0.55
Acyl chain length
E
Spearman correlation test:
p-value = 0.44
Number of double bounds

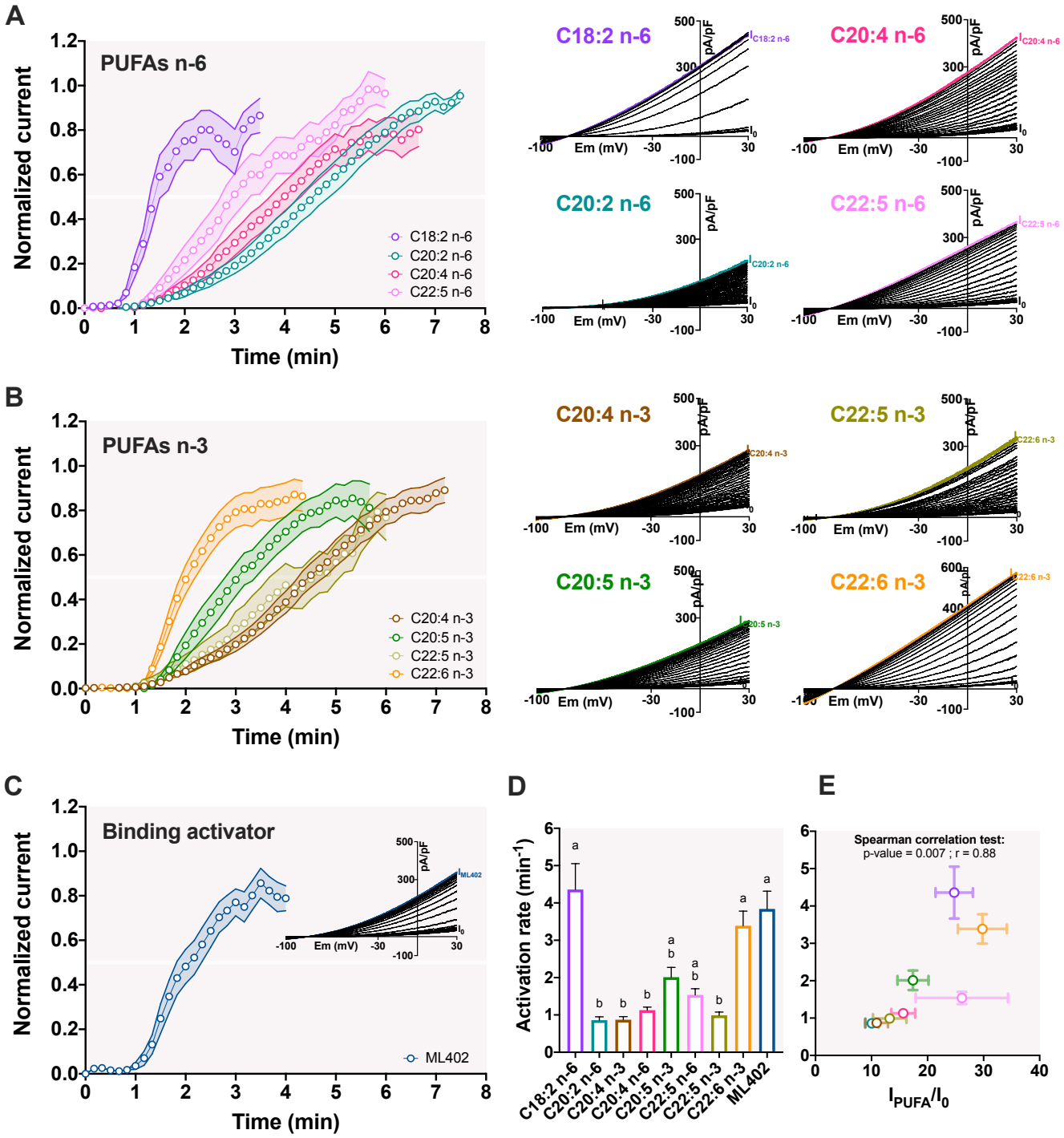
A
PUFAs n-6
Normalized current
Time (min)
C18:2 n-6
C20:2 n-6
C20:4 n-6
C22:5 n-6
C18:2 n-6
C20:4 n-6
C20:2 n-6
C22:5 n-6
pA/pF
Em (mV)
B
PUFAs n-3
C20:4 n-3
C20:5 n-3
C22:5 n-3
C22:6 n-3
C20:4 n-3
C22:5 n-3
C20:5 n-3
C22:6 n-3
C
Binding activator
ML402
D
Activation rate (min-1)
C18:2 n-6
C20:2 n-6
C20:4 n-3
C20:4 n-6
C20:5 n-3
C22:5 n-6
C22:5 n-3
C22:6 n-3
ML402
E
Spearman correlation test:
p-value = 0.007 ; r = 0.88
IPUFA/I0

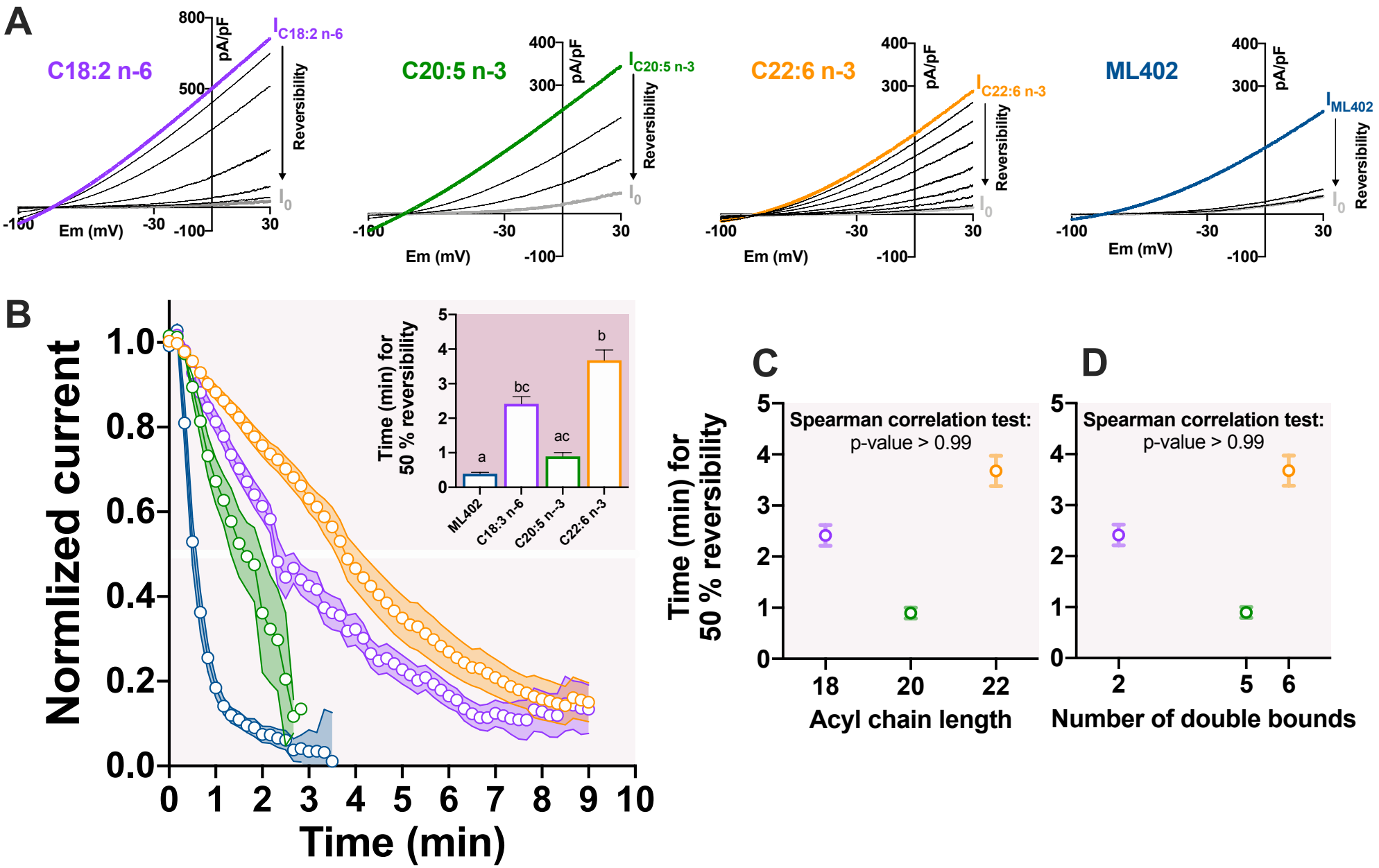
A
C18:2 n-6
800
500
pA/pF
I C18:2 n-6
Reversibility
I0
-100
Em (mV)
-30
-100
30
C20:5 n-3
400
300
pA/pF
I C20:5 n-3
Reversibility
I0
-100
-30
30
Em (mV)
-100
C22:6 n-3
400
300
pA/pF
I C22:6 n-3
Reversibility
I0
-100
-30
30
Em (mV)
-100
ML402
400
300
pA/pF
I ML402
Reversibility
I0
-100
-30
30
Em (mV)
-100
B
Normlized current
1.0
0.8
0.6
0.4
0.2
0.0
0 1 2 3 4 5 6 7 8 9 10
Time (min)
Time (min) for 50 % reversibility
5
4
3
2
1
0
a
bc
ac
b
ML402
C18:3 n-6
C20:5 n--3
C22:6 n-3
C
D
Time (min) for 50 % reversibility
Spearman correlation test:
p-value > 0.99
18
20
22
Acyl chain length
Spearman correlation test:
p-value > 0.99
2
5
6
Number of double bounds

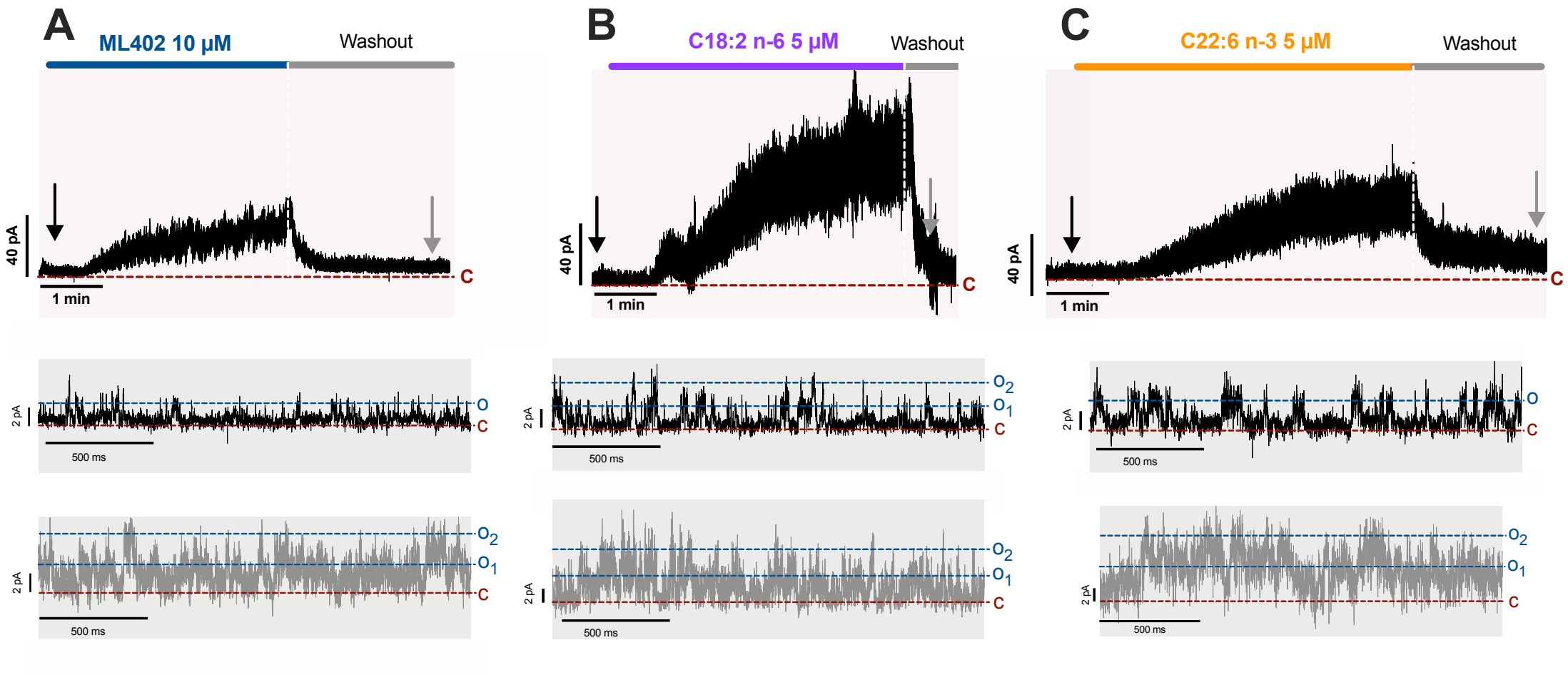
A
ML402 10 μM
Washout
40 pA
1 min
C
2 pA
500 ms
O
C
O2
O1
C
B
C18:2 n-6 5 μM
Washout
40 pA
1 min
C
2 pA
500 ms
O2
O1
C
C
C22:6 n-3 5 μM
Washout
40 pA
1 min
C
2 pA
500 ms
O
C
O2
O1
C

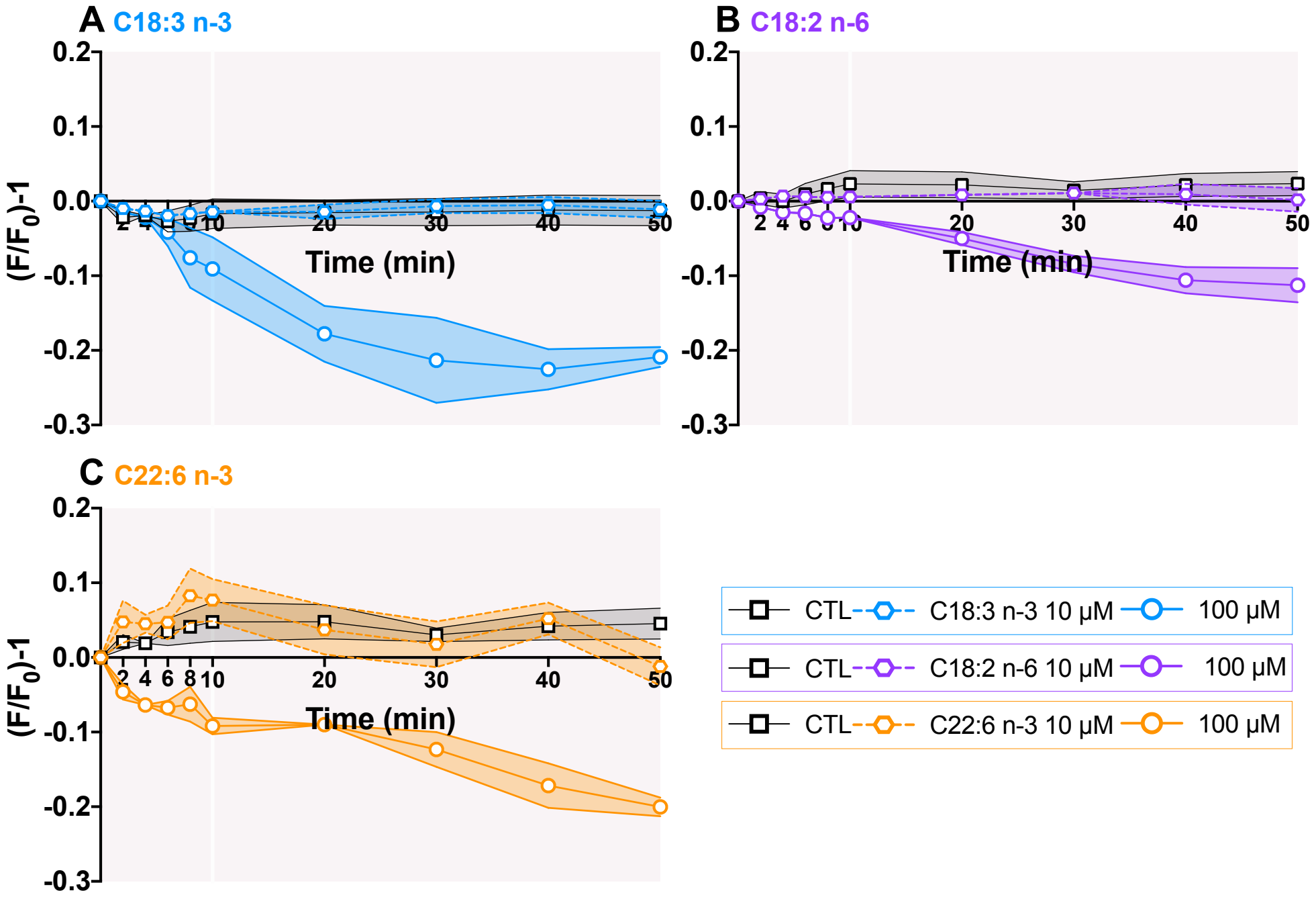
A C18:3 n-3
B C18:2 n-6
C C22:6 n-3
(F/F0)-1
Time (min)
0.2
0.1
0.0
-0.1
-0.2
-0.3
2 4 6 8 10 20 30 40 50
CTL
C18:3 n-3 10 μM
100 μM
C18:2 n-6 10 μM
C22:6 n-3 10 μM

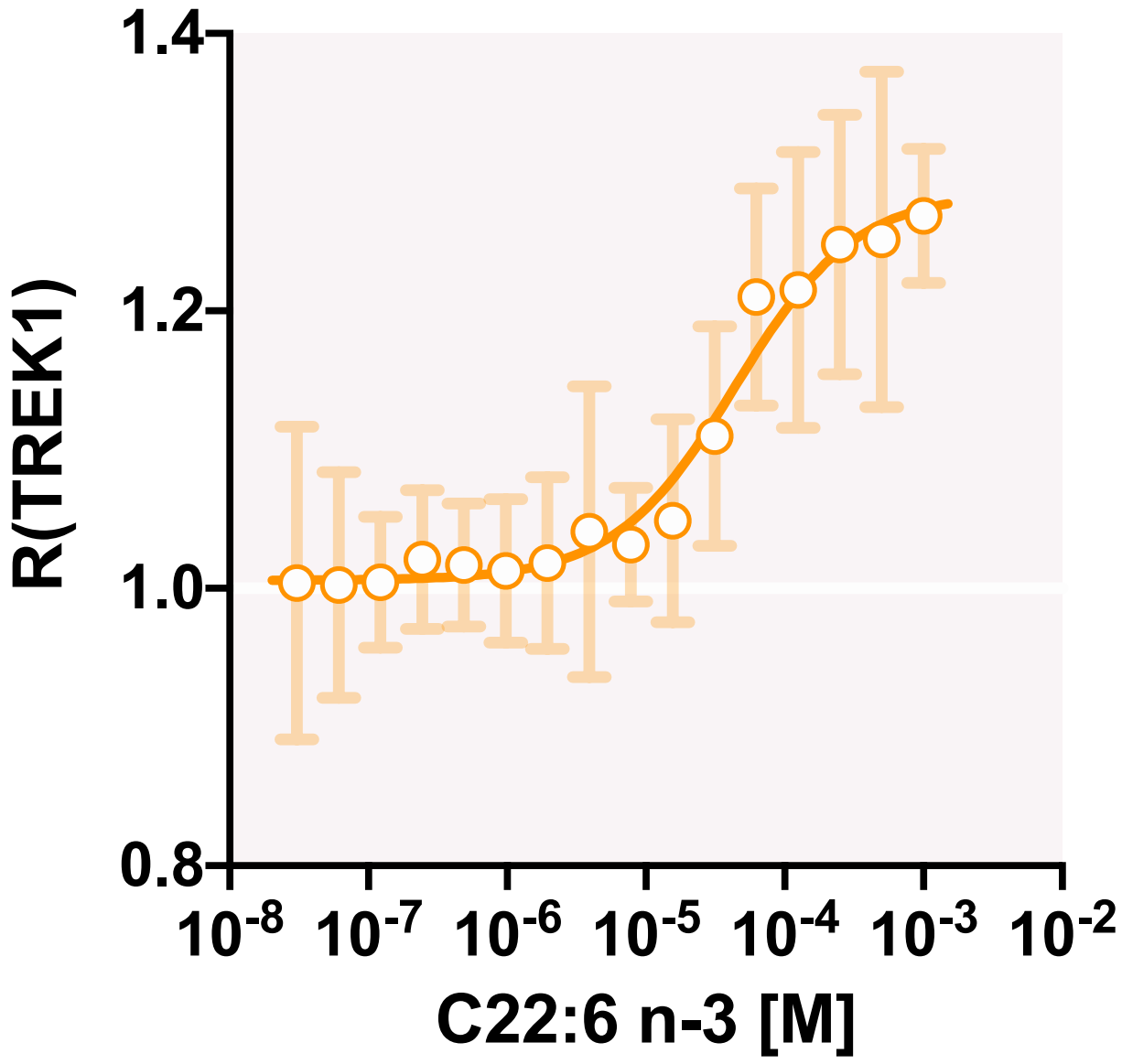
1.4
1.2
1.0
0.8
R(TREK1)
10-8
10-7
10-6
10-5
10-4
10-3
10-2
C22:6 n-3 [M]